

# Footprint-based biometric verification

Andreas Uhl and Peter Wild\*  
Department of Computer Sciences  
University of Salzburg, Austria

We investigate the potential of foot biometric features based on geometry, shape and texture and present algorithms for a prototype rotation invariant verification system. An introduction to origins and fields of application for footprint-based personal recognition is accompanied by a comparison with traditional hand biometry systems. Image enhancement and feature extraction steps emphasizing on specific characteristics of foot geometry and their permanence and distinctiveness properties, respectively, are discussed. Collectability and universality issues are considered as well. A visualization of various test results comparing discriminative power of foot shape and texture is given. The impact on real-world scenarios is pointed out, and a summary of results is presented.

Keywords: Biometrics, Verification, Footprint, Eigenfeet, Foot geometry.

## I. INTRODUCTION

Among the numerous biometric techniques used for human identification, foot biometry has been largely neglected so far. Even though the human foot has been extensively studied in medical and forensic research [6] and obviously bears similar distinctive properties like the human hand, its use in commercial biometric systems is considered complicated. Reasons include a nonhabituated environment, user-unfriendly data acquisition (due to the practice of wearing shoes) and, last, uncomfortable associations at the acquisition step. By tradition in Arab countries, it is considered offensive to show someone the sole of your foot.

Most access control systems rely on face, fingerprint, hand geometry, iris, palmprint and signature features (see [3]), and in the future many more business applications (e.g. banking) will employ biometric identification. While some biometric features are not secret and may be generated out of publicly available data, it is in each user's interest that private biometric features such as retina or even fingerprints are not compromised. However, precisely because foot biometry is not and probably will never be a suitable authentication mechanism for high-security applications, storage of foot biometric features does not necessarily imply security threats.

If the environment allows user-friendly data acquisition, e.g., thermal baths, or security issues demand uncritical features, foot biometry may be considered as a useful alternative. Within special environments, foot biometry might even be implemented as a covert system in contrast to hand biometric techniques. Therefore, the image acquisition step used in this work is inherently simple, and it does not employ any special illumination, nor does it use pegs to cause any further inconvenience.

The first footprint-based recognition dates back to Kennedy [6] in the late 1980s, who used inked bare-foot impressions to extract 38 local geometrical features,

such as length between heel and tips of toes, optical centers of heel and toes or width of ball and heel. While Kennedy's work concentrated on forensic applications, the first scheme concentrating on footprint-based authentication using simple Euclidian distance between footprints was introduced by Nakajima et al [11]. Operating on pressure distribution data and simple Euclidian distance, recognition rates of 85% could be achieved. Further work concentrates on static and dynamic footprint-based recognition using hidden Markov models [4, 5] with recognition rates of about 80 to 97.8% dependent on feature selection and database size. Since neither taking ink-based impressions in the first case nor recognition rates of 80 to 85% are suitable for commercial security applications, we investigate more elaborate approaches to foot biometrics. While the idea of using shape and skin texture information of the human hand is not new and numerous biometric features are described in detail in [7, 17, 18], we examine the application of some of these features in foot biometrics. Traditional hand biometric features are most likely to be applicable to foot biometrics; thus, we investigate their discriminative properties. However, techniques also used in face recognition (e.g. Eigenfaces as described in [16]) can be successfully implemented. Second, a goal of this paper is the introduction of a prototype footprint verification system. Implemented biometric measurements involve:

- Shape and geometrical information focusing on characteristics such as length, shape and area of the silhouette curve, local foot widths, lengths of toes, and angles of inter-toe valleys;
- soleprint features analogous to palmprint-based verification extracting texture-based information of the sole of the foot;
- minutiae-based ballprint features employing different techniques used in fingerprint verification systems;
- Eigenfeet features (corresponding to Eigenfaces in traditional face recognition) in the principal com-

---

\*Electronic address: uhl,pwild@cosy.sbg.ac.at

ponent subspace for recognition of both shape and textural information.

A short introduction to hand and finger biometric features and their application in foot biometrics will be given in the first part of this paper. Section II describes the overall system architecture and explains the various normalization and image enhancement steps. Various implemented features and how they can be extracted from a normalized foot-image is presented in detail in Sec. III. How to perform matching is presented in Sec. IV. Experimental setup and test results are presented in Sec. V, and the impact of results for real-world setups is analyzed. This includes a description of several advantages and disadvantages of the introduced foot biometry system. Last, Sec. VI presents our conclusions.

## II. SYSTEM SETUP

There are numerous biometric systems providing personal verification based on hand images. Since capturing and normalization of *dorsal* (towards the upper surface) foot images in real-world scenarios is rather complicated and makes it difficult to implement a covert system, we limit our observation to *plantar* (opposite of dorsal) foot biometric systems and *palmar* (towards the palm) hand biometrics respectively. All such systems have in common a less complex image acquisition step. Images can be captured by flatbed scanners or cameras at a low resolution rate starting at 45 dpi [18]. Although hand geometry-based metrics do not vary significantly across different people [3], they can nevertheless be used for the verification task.

We have designed an image-based multimodal footprint verification system using input images with 256 grey levels of an HP 3500c flatbed scanning device as the single sensor operating at 600dpi resolution. The scanner supports an area of  $216 \times 297$  mm resulting in  $5102 \times 7016$  input images, which was found to be sufficient for single foot captures. In order to provide each of the different feature extractors with adapted image resolutions, bilinear downsampling is applied. Like most other biometric systems (see e.g. [7],[14]) the proposed foot-biometric authentication system consists of separate modules for *preprocessing*, including image registration and enhancement, *feature extraction* (details are described in Sec. III); and *matching* (see Sec. IV).

### A. Preprocessing

Preprocessing is important for reliable foot recognition. Nakajima et al. [11] could improve their Euclidian-distance-based footprint recognition method on raw images from roughly 30% to 85% by just achieving normalization in direction and position. While for unconstrained hand images a re-alignment of individual fingers

using texture blending [17] is promising, an adaption to foot biometrics is considered complicated due to close-fitting toes and has not yet been implemented. However, a successful alignment of toes could further increase recognition rates of global features. So far, in the preprocessing stage the following steps are executed:

1. Binarization using Canny edge detection and thresholding.
2. Rotational alignment using statistical moments.
3. Displacement alignment restricting the image to the bounding box of the footprint.

Last, background pixels are masked and the processed footprint is scaled to provide each of feature extractors with appropriate resolution input. While most of the introduced feature extractors (Silhouette, Shape, Toe-Length, SolePrint) demand an aligned  $512 \times 1024$  footprint image as input, the Eigenfeet algorithm works on a subsampled low resolution  $128 \times 256$  and minutiae extraction is performed on the maximum 600-dpi version.

#### 1. Binarization

In order to preserve edges for accurate shape feature extraction, we first employ Canny edge detection [1] with binary thresholding on the original image  $B$  to keep the most significant edges only, which reliably represent foot contours. Then, within the obtained image  $B_1$  we fill the interior of the foot using binary thresholding on  $B$ , i.e.  $B_2(x, y) = \max(\text{bin}_b(B)(x, y), B_1(x, y))$  where  $\text{bin}_b(B)$  denotes the binarization of  $B$  using threshold  $b$ . This binarized image  $B_2$  is next subjected to morphological dilation using a square structuring element  $S$  to close the boundary:

$$B_3 = B_2 \oplus S = \{(x, y) | S_{xy} \cap B_2 \neq \emptyset\} \quad (1)$$

where  $S_{xy}$  denotes a shift of  $S$  by  $(x, y)$ . This operation is followed by a removal of small white 4-connected binary large objects (BLOBs) and a filling of all black BLOBs except the background to get the binarized image  $B_4$ . Last, we employ morphological erosion on this image:

$$B_5 = B_4 \otimes S = \{(x, y) | S_{xy} \subseteq B_4\}. \quad (2)$$

#### 2. Rotational alignment

To achieve rotational alignment, we match the footprint with the best-fitting ellipse, as described in [15]. This method has been used in face recognition [2] and hand recognition systems [7] and has proven to be successful also for alignment of footprints [11]. The goal is to estimate the angle  $\Theta$  between  $y$ -axis and the major axis of the best matching ellipse. Having extracted the center of mass  $C = (\bar{x}, \bar{y})$  (which is also the center of the

ellipse, see Sec. III) and letting  $x' = x - \bar{x}$  and  $y' = y - \bar{y}$ , then the angle  $\Theta$  of inclination is given by:

$$\Theta = \frac{1}{2} \arctan\left(\frac{2\mu_{1,1}}{\mu_{2,0} - \mu_{0,2}}\right) \quad (3)$$

$$\mu_{2,0} = \sum_{i=1}^n \sum_{j=1}^m (x'_{ij})^2 B(i, j) \quad (4)$$

$$\mu_{1,1} = \sum_{i=1}^n \sum_{j=1}^m x'_{ij} y'_{ij} B(i, j) \quad (5)$$

$$\mu_{0,2} = \sum_{i=1}^n \sum_{j=1}^m (y'_{ij})^2 B(i, j) \quad (6)$$

### III. FEATURE SELECTION

To cope with unacceptable False Acceptance Rates (FARs) and False Rejection Rates (FRRs), we design a *multimodal* foot biometric system [13] in the sense of combining different representation and matching algorithms in order to improve recognition accuracy. Therefore, we observe hybrid approaches and even extend our considerations to fingerprint biometrics since typical ridge structures are also present on large parts of the foot.

#### A. Classification According to Feature Selection

According to [17] common hand biometric systems and therefore foot biometric systems can be classified in an analogous manner as follows:

- Schemes relying on geometric features comprising silhouette shape and the lengths and widths of fingers, among others;
- Palmprint-based verification systems extracting palm curves;
- Hybrid approaches (such as [7]) employing fusion at the feature extraction, matching-score, or decision level to improve error rates.

Additionally, a lot of systems concentrating on fingerprint verification exist (such as the NFIS2 minutiae-matching software from NIST [12]). However, fingerprint matching results are fused with hand geometry in multiple biometric schemes [13] rather than combined employing a single sensor [8]. A reason for this might be that, usually, fingerprint matching requires special hardware for image acquisition and does not work on low-resolution input. Nevertheless, when ridge structures can successfully be extracted from the captured scans of palms or feet, system performance can be increased using fusion without the cost of additional sensors or further inconvenience caused by multiple-step data acquisition.

In the next few paragraphs, we introduce possible foot biometric features and how they can be derived from their hand biometric counterparts. Furthermore, we point out problems concerning feature extraction due to anatomical differences between hand and foot and analyze possible resorts.

#### B. Geometric Features

Geometric measurements are frequently employed in hand biometric systems due to their robustness to environmental conditions, and a large number of possible features fall into this category. Considering the sole of the foot to be prone to injuries, shape-based features seem also well suited for the foot verification task. However, due to different spreadings of toes, we expect a rather high intra-personal variability in general. One reason for this is that many hand recognition schemes rely on a robust identification of finger tips and finger valleys. When interfinger valleys cannot be detected reliably, a normalization, i.e., correct placement of individual fingers, is hard to achieve. The extraction of these characteristic landmarks is often facilitated by pegs [14], while more advanced schemes like [18] are peg-free but demand high contrast between background and palm. Since an introduction of pegs is unacceptable for the image acquisition step, and spread toes are not the default case, the reliable detection of inter toe valleys deserves closer attention in foot biometrics. Regardless the expected weak performance of shape features, we try to map both global features (focusing on palm width, length or hand area) and local features (representing, e.g., finger lengths and widths at various positions) to their counterparts in foot biometrics.

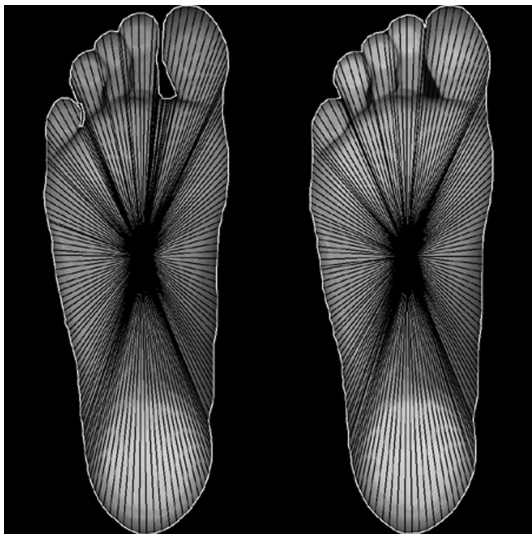
A list of implemented features for the foot-shape-based verification task can be found in Table I.

##### 1. Silhouette

In addition to the height and width of the foot as recordable features, which can obviously be derived analogously to hand geometry, the first feature to be introduced focuses on the contour polygon. Silhouette geometry is used in [18] to construct a feature vector projecting contour points in two dimensions onto the eigenspace spanned by the 40, 100, 200 or 400 most-significant eigenvectors of covariance matrix  $\mathbf{C}$  obtained by a set of sample hand contours. While at first glance, the idea of applying the same scheme in foot biometrics is promising, the alignment of toes in a preferred direction in order to be able to capture the correct silhouette for matching is troublesome. For this reason, we apply a rather simple feature extraction and use dynamic time warp in the matching stage to cope with missing parts in the contour polygon. That is, we compute distances  $s_k = |S_k - C|$  for  $k \in \{1, \dots, l(S)\}$ , where  $S = \{S_1, S_2, \dots, S_{l(S)}\}$  is

Algorithm	Features	Classifier
Silhouette	Contour distance to centroid, length and enclosed area of silhouette polygon	Dynamic time warp matching
Shape	15 local foot widths and positions	Based on Manhattan distance
ToeLength	5 toe lengths and 4 intertoe angles	Based on weighted Euclidian distance
Soleprint	Variance of 288 overlapping blocks in edge-detected image (similar to [7])	Based on Euclidian distance
Eigenfeet	Projection of subsampled footprint onto feature space spanned by 20 most-significant principal components	Based on Manhattan distance
Minutiae	Using the NIST [12] <code>mindtct</code> minutiae extractor on ballprint region under the big toe	Based on NIST [12] <code>bozorth</code> matcher

TABLE I: Employed geometric and texture-based features

FIG. 1: Silhouette: Rejected genuine attempt ( $m_1 = 0$ ) due to slightly spread toes.

the silhouette polygon at appropriate sampling rate,  $C$  is the center-of-mass, and  $L(S)$ ,  $A(S)$  are the length and enclosed area, respectively, of the silhouette polygon, to obtain our feature vector  $f_1 = (s_1, \dots, s_{l(S)}, L(S), A(S))$ . Having a binary image  $B$  of size  $n \times m$  and letting  $A$  be the number of white pixels representing the foot, then  $C = (\bar{x}, \bar{y})$  can be determined as follows:

$$\bar{x} = \frac{1}{A} \sum_{i=1}^n \sum_{j=1}^m jB(i, j), \quad \bar{y} = \frac{1}{A} \sum_{i=1}^n \sum_{j=1}^m iB(i, j) \quad (7)$$

Figure 1 illustrates the silhouette polygons of two samples acquired from the same user.

## 2. Shape

While the shape of the human wrist is often neglected in biometric systems, the actual shape of the foot is char-

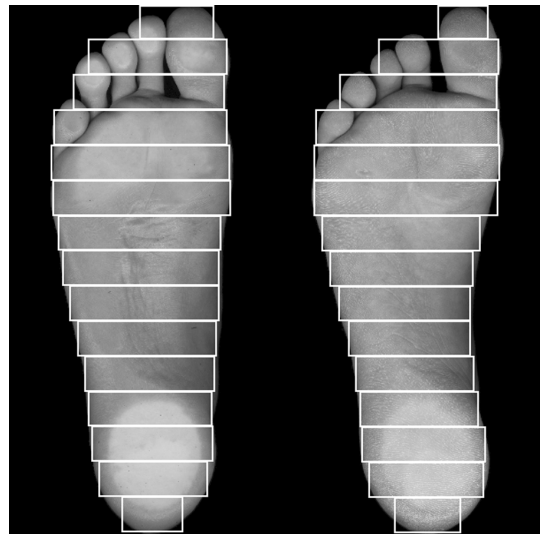


FIG. 2: Shape: Imposter attempt.

acterized by its local widths and bending. The next feature is an approach that takes this fact into account (see Fig. 2). After aspect ratio preserving normalization of the footprint in order to achieve predefined rotation and size, the foot is divided into  $N$  vertical slices  $V_0, \dots, V_{N-1}$  with equal dimensions. The y-monotone polygon  $S_y$  is now used to compute the average width of the foot per slice, i.e. the average width  $w_i$  of the set  $V_i \cap S_y$  for  $i \in \{0, \dots, N-1\}$  of in-foot pixels. Using a binary representation  $B$  of size  $n \times m$  and the characteristic function  $\chi$ , we get:

$$w_i = \frac{N}{n} \sum_{j=1}^n \sum_{k=1}^m \chi_{V_i \cap S_y}(j, k) \quad (8)$$

The final feature vector is now constructed as  $f_2 = (w_2, \dots, w_{N-1})$ , with  $N = 15$ . We neglect the first two slices to suppress noise caused by toes. A significant problem concerning foot shape mentioned in [11] is the fact that feet are generally about 5 mm larger in the evening than in the morning due to hypostatic conges-

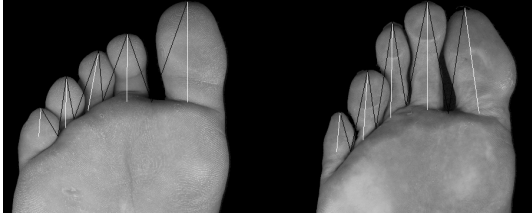


FIG. 3: ToeLength: Imposter attempt.

tion. Also a significant change in weight may cause high intrapersonal variability.

### 3. ToeLength

Hand extremities, i.e., the finger tips and the finger valleys, are typically exploited using a binary representation of the input image and deriving a different number of features. Kumar et. al. [7] for example, use 12 hand extremity features including 4 finger lengths, 8 finger widths (2 widths per finger). Sanchez-Reillo et. al. [14] use even more local finger widths, namely 25 features. More recent schemes [18] employ an extraction of contour shape information for individual fingers and incorporate principal component analysis and/or independent component analysis for the construction of the feature vector. Mapping hand extremity features to toes in foot biometrics is promising, but a crucial problem is that in unstrained pose, toes are close to each other. Thus a simple binary thresholding using Otsu's Method, as in [7], will not suffice in general. Instead, we employ both binarization and a Canny Edge detection [1] algorithm to first find candidate points for toe valleys by detecting the entrance between two toes. Then candidate points are improved by following the edge separating two toes within a cone centered in the center of mass of the binary foot image. We then extract 9 toe extremity values, comprising the 5 toe lengths and the 4 intertoe angles as depicted in Fig. 3, to construct the feature vector  $f_3 = (L_1, \alpha_1, L_2, \alpha_2, L_3, \alpha_3, L_4, \alpha_4, L_5)$ .

An interesting convenience having extracted the length of the big toe and its neighboring one is a preclassification of feet. Just as fingerprints can be separated into basic pattern-level classes known as *arch*, *left loop*, *right loop*, *scar*, *tented arch*, and *whorl* [12], it is possible to classify feet according to the differences in length of *hallux* and second toe into *egyptian* (hallux longer than second toe), *greek* (second toe longer than hallux) and *square* (both toes have almost the same length) feet. Orthopaedic surgeon Morton [9] was the first to describe this phenomenon of the second toe (also called *Morton's toe*) being longer than the great toe as a part of Morton's syndrome.

## C. Texture-Based Features

Skin-texture-based identification on palmprints involves the challenge of extracting line structures. Using feet instead of hands a new problem arises, since typical principal lines are not present. Instead a comb-like pattern is visible, which seems to be sensitive to different pressure distributions. For this reason, we apply a simpler generic but robust method [7] to extract texture-based patterns. While line information is extracted at lower resolution using directional Prewitt edge detection, typical ridge structure is also present in the footprint at high resolutions even if no special ridge extraction device such as a fingerprint scanner is used. For this reason, we incorporate a minutiae based feature extraction step developed for fingerprint matching [12] estimating local ridge structure on a specified part of the 600dpi input image. Last, both shape and texture information are processed using principal component analysis [16] at lowest resolution rate. Table I lists the incorporated texture-based features Soleprint, Eigenfeet and Minutiae.

### 1. Soleprint

In cooperative environments, e.g., access control in thermal baths, we expect intraclass pressure distribution to exhibit low variance. Additionally, for hand biometrics, Kumar et al. [7] report their texture-based feature to outperform their introduced geometric scheme. However, due to less distinctive line structures, dorsal injuries, textile defilement, and skin creases caused by touching the scanning device, it is not clear whether this general statement also holds for foot biometrics. For this reason, we apply their classical palmprint-based feature extraction step to foot biometrics and later on compare its matching performance.

After rotational alignment, Kumar et al. [7] extract a square palmprint region  $R_p$  of fixed size  $s_p \times s_p$  centered at the center-of-mass  $C_p$  such that the square is completely inscribed the palm. While the palm is identifiable as a square region, the part of the foot which constitutes the sole image used for feature extraction is yet to be determined. Letting  $F$  denote the binary  $n \times m$  footprint and  $n = h(F)$  be the height of the foot, we have chosen the largest inscribed rectangle  $R \subset F$  with height  $a$  and length  $b$  such that:

$$a = \frac{3h(F)}{5}, R \cap \{(x, y) | y < \frac{h(F)}{5} \vee y > \frac{4h(F)}{5}\} = \emptyset. \quad (9)$$

We then scale the extracted region  $R$  to predefined size  $300 \times 600$  pixel, which is twice the size of  $R_p$ . Then we normalize  $R$  to predefined mean  $\phi_d$  and variance  $\rho_d$  as in [7]. We have chosen  $\phi_d := 100$  and  $\rho_d := 200$ . All new pixel values  $R'(x, y)$  fulfill:

$$R'(x, y) := \begin{cases} \phi_d + \lambda & \text{if } R(x, y) > \phi, \\ \phi_d - \lambda & \text{else.} \end{cases} \quad (10)$$

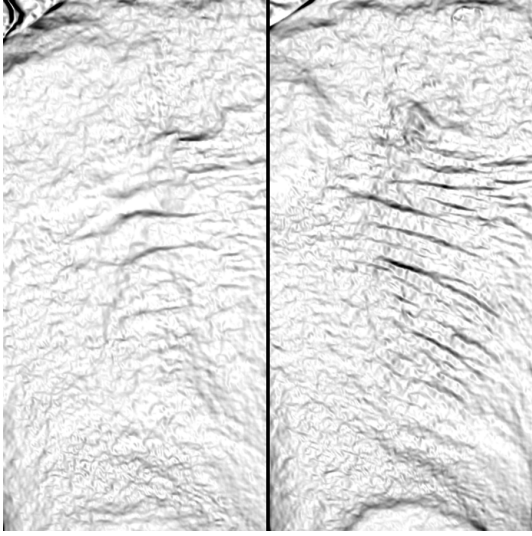


FIG. 4: Soleprint: Rejected genuine attempt ( $m_2 = 7$ ) due to creases in rotated sole.

where

$$\lambda = \sqrt{\frac{\rho_d(R(x, y) - \phi)^2}{\rho}}. \quad (11)$$

For line and crease detection of the sole, we employ  $5 \times 5$  Prewitt kernels  $p_i$  in different directions (0 deg, 45 deg, 90 deg, and 135 deg) and get accumulated edges (see Fig. 4):

$$K(x, y) = \max\{R_1(x, y), \dots, R_4(x, y)\} \quad (12)$$

where  $R_i(x, y) = p_i * R'(x, y)$ , i.e., the normalized footprint is convoluted with each of the Prewitt kernels. The actual feature vector  $f_4 = \{\sigma_1^2, \dots, \sigma_{288}^2\}$  consists of an extraction of variances of 288 overlapping blocks, each of size  $24 \times 24$  pixels.

## 2. Eigenfeet

The motivation behind the Eigenfeet feature, which is derived from *Eigenfaces*, introduced by Turk and Pentland [16], is a method based upon the most relevant features for classification instead of an arbitrary selection of features. The main idea is to think of an image  $\Gamma$  as an  $m \times n$ -dimensional vector that can be represented exactly in terms of a linear combination of principal components, i.e., eigenvectors (also called Eigenfaces for facial images), computed on the covariance matrix of training images. Eigenvectors are ordered according to eigenvalues and only the ones with the  $M$  highest eigenvalues are kept, leaving the most-important features that are critical for the recognition task. Feature extraction using the Eigenfeet algorithm is equal to projecting the  $128 \times 256$  input image onto the *feet space* spanned by the 20 most significant eigenvectors depicted in Fig. 5 obtained by a



FIG. 5: Eigenfeet: Computed eigenfeet of 20 footprints.

set of also 20 training images. Thus, in the strict sense, the Eigenfeet feature is a both texture-based and shape-based approach, since foot silhouette information is also encoded within eigenvectors. Matching involves a simple distance metric in foot space with thresholding.

A computation of Eigenfeet, which precedes enrollment and matching, involves the following two tasks [16]:

1. Acquisition of an initial training set of centered  $m \times n$  foot images represented as vectors  $\Gamma_i$  for  $i \in \{1, \dots, M\}$ , from which the average foot vector  $\Psi$  is subtracted:

$$\Phi_i = \Gamma_i - \Psi, \quad \Psi = \frac{1}{M} \sum_{i=1}^M \Gamma_i \quad (13)$$

2. Computation of  $mn \times mn$  covariance matrix:

$$\mathbf{C} = \frac{1}{M} \sum_{i=1}^M \Phi_i \Phi_i^T = \mathbf{A} \mathbf{A}^T \quad (14)$$

and eigenvectors  $u_k$  with according eigenvalues  $\lambda_k$ . For computational efficiency, often the  $M \times M$  Matrix  $\mathbf{A}^T \mathbf{A}$  is used instead, since the  $M$  eigenvectors  $v_k$  of  $\mathbf{A}^T \mathbf{A}$  correspond to the  $M$  largest eigenvalues  $u_k$  of  $\mathbf{A} \mathbf{A}^T$  fulfilling the equation  $u_k = \mathbf{A} v_k$  and usually  $M$  is much smaller than  $mn$ .

3. Ordering and selection of the  $L$  highest eigenvectors with corresponding eigenvalues.

Having selected a set of Eigenfeet  $u_i$  with  $i \in \{1, \dots, L\}$  and average foot  $\Psi$ , feature extraction comprises the following steps:

1. Normalization of the foot vector  $\Gamma$  calculating  $\Phi = \Gamma - \Psi$ .
2. Projection onto eigenspace to get the feature vector components  $\omega_i = u_i^T \Phi$ . The feature vector consists of exactly  $L$  components  $f_5 = (\omega_1, \dots, \omega_L)$  such that  $\Phi$  is approximated by:

$$\Phi \sim \sum_{i=1}^L \omega_i u_i \quad (15)$$

Last, matching is executed using Manhattan distance.



FIG. 6: Minutiae: A typical ballprint region containing 300 to 400 minutiae.

### 3. Minutiae

We use the NFIS2 [12] minutiae extraction and matching software MINDTCT and BOZORTH3 to extract minutiae information out of the ballprint region under the big toe. After rotational alignment, we extract a rectangular region of fixed size  $\frac{h}{6} \times \frac{w}{2}$  centered at  $B = (\frac{3w}{4}, \frac{3h}{12})$ , where  $h$  and  $w$  are the height and width of a bounding box circumscribing the input footprint. We then employ contrast-improving histogram stretching on the extracted region, which is still at 600-dpi resolution. While MINDTCT binarizes this input image and detects up to 400 minutiae per ballprint image (depending on image quality, see Figure 6), BOZORTH3 is employed at the classification stage operating in 1:1 comparison mode.

## IV. MATCHING

Since we incorporate multiple biometric features, there are several possible *information fusion* mechanisms for matching according to [13], namely (1) fusion at feature extraction level, (2) fusion at matching score level, and (3) fusion at decision level. We examine both (2) using a weighted sum of matching scores and (3) using a majority vote scheme.

Most of the employed algorithms (Shape, ToeLength, SolePrint, Eigenfeet) use (weighted) Euclidian or Manhattan distance between the user's feature vector  $f$  and the claimed identity's reference vector  $t$  for classification, see Table I. The incorporated BOZORTH3 matcher for the Minutiae feature already outputs a matching score, and the Silhouette algorithm differs in the way that an evaluation function  $e$  is used. For all  $1 \leq i \leq n$ , we let  $f[i]$  denote the  $i$ -th element of  $f$  and let  $t[j]$  be the  $j$ -th ( $1 \leq j \leq m$ ) element of the reference template, and we

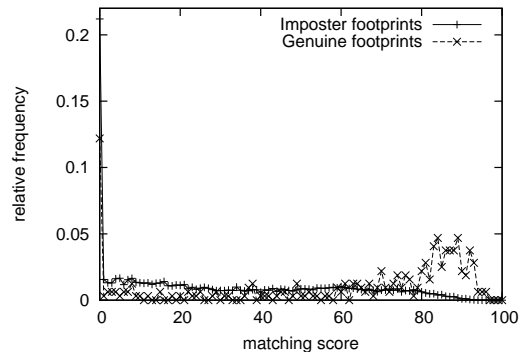


FIG. 7: Silhouette: Genuine and imposter distributions.

then define:

$$e(f, t) = \alpha D(f, t) + \beta |f[n-1] - t[m-1]| + \gamma |f[n] - t[m]|, \quad (16)$$

where  $D$  compares silhouette data sets using dynamic time warping (DTW) [10] with a cost function  $c(i, j) = (f[i] - t[j])^2$ . Dynamic time warping computes an optimal match between  $f$  and  $t$  using:

$$d(i, j) := \begin{cases} 0, & \text{if } i = 1, j = 1 \\ c(i, j) + d(i-1, 1), & \text{if } i > 1, j = 1 \\ c(i, j) + d(1, j-1), & \text{if } i = 1, j > 1 \\ c(i, j) + \min(d(i-1, j), d(i, j-1)), & \text{else.} \end{cases} \quad (17)$$

The minimum distance between both data sets is  $D(f, t) = d(n, m)$ .

Last, for each algorithm a discrete matching score  $m_i \in \mathbb{N} \cap [0, 100]$  for  $1 \leq i \leq 6$  is calculated.

## V. EXPERIMENTAL RESULT

We investigate achievable recognition accuracy and both inter- and intraclass variability of single incorporated foot biometric features examining distributions of genuine and imposter footprints diagrammed in Figures 7-12. We understand the *genuine distribution* as being the distribution of scores generated from pairwise comparisons of samples from the same person, while samples from different persons contribute to the *imposter distribution*. Different algorithms are compared using False Match Rate (FMR) and False Non Match Rate (FNMR) at different thresholds  $t$  depicted in the form of a Receiver Operating Characteristics (ROC) Curve in Figure 13. Last, we try to analyze matching performance results.

### A. Test Setup

The experiments were conducted by using our database of 135 male and 25 female footprints of 32 volunteers aged

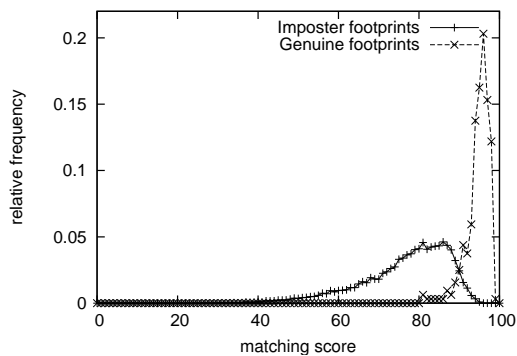


FIG. 8: Shape: Genuine and imposter distributions.

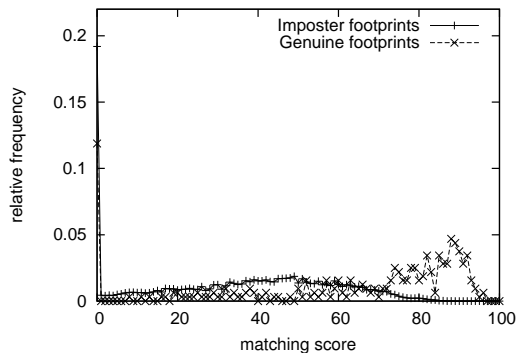


FIG. 9: ToeLength: Genuine and imposter distributions.

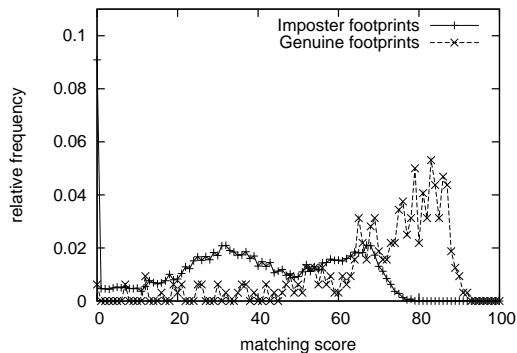


FIG. 10: Soleprint: Genuine and imposter distributions.

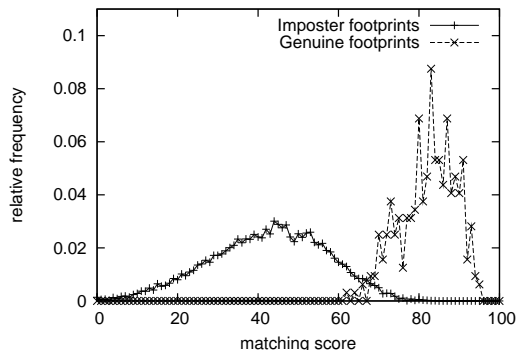


FIG. 11: Eigenfeet: Genuine and imposter distributions.

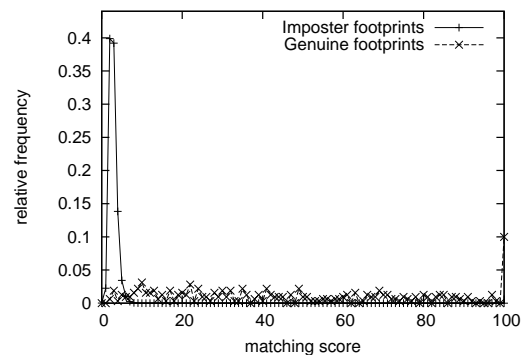


FIG. 12: Minutiae: Genuine and imposter distributions.

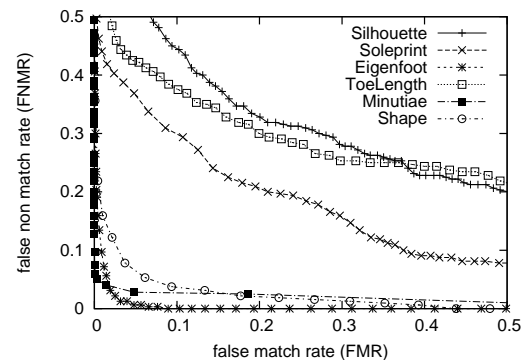


FIG. 13: Comparing Receiver Operating Characteristics.

20 to 40. Each of the 5 acquired footprint samples of the right foot per user was recorded with the user sitting in front of the scanning device. Thus, the footprints are not heavily loaded with full weight. Image capturing is preceded by a cleaning of scanning device and sole. In order to minimize the influence of environmental light, all samples were captured in a shaded room within a time span of 15 min per user. It is clear, that both small member database size and short time span yields weak results for real-world applications. However, the absence of large-scale publicly available footprint databases is an open problem. ([11] use 110 samples of 11 users over the period of 1 month, [4] use 300 samples of 5 users captured at the same time for testing.) The acquired test dataset does not include any of the 20 images used for computing the predefined *Eigenfeet* matrix, and only two persons are recorded in both sets. To get an impression of inter and intra-class variability concerning the employed features, we executed 320 genuine attempts (each footprint was matched against the remaining images of the same foot) and 12,400 imposter attempts on the test set.

## B. Matching Performance

In order to compare matching performance we have selected for each algorithm the operating point with closest distance to the first median, i.e., which is closest to a vir-

tual operating point yielding Equal Error Rate (EER, the value such that  $FAR = FRR$ ).

The first feature to be analyzed is the Silhouette algorithm. As we have expected, silhouette shape is a volatile feature and shows an extremely high EER of about 29% due to the large overlap between genuine and imposter distributions, as shown in Fig. 7. An interesting phenomenon is the large amount of genuine footprints achieving the lowest score 0 due to the sensitivity to spread toes, as can be seen in Fig. 1. This results in high intrapersonal variability even though dynamic time warping is employed. Compared to other features listed in Fig. 13, Silhouette and ToeLength are the worst performing algorithms.

For the Soleprint feature, we first expected matching results similar to palmprints in the hand biometric case. But whereas Kumar et al. [7] achieve a FAR of 4.49% and an FRR of 2.04%, we observe rates to be an order of magnitude higher (FMR 19.5% and FNMR 20.94%) in the foot biometric case. Besides the absence of typical expressive lines, creases (often appearing in rotated footprints, see Fig. 4 for an example) constitute a significant problem. Another challenge is textile defilement due to the practice of wearing socks, which was avoided in advance by cleaning the sole before image acquisition.

The Eigenfeet feature proved to be most suitable for footprint-based personal recognition. It does not need highly resolved input images and compared to other footprint-features it uses small-size feature vectors of 160 bytes. Its accuracy performance of FMR 2.52%, FNMR 2.18% is quite competitive and can be compared with results from hand biometry systems [7, 14]. But the effect of training set size and time lapses between recordings on verification performance is yet to be analyzed.

Using length of toes and intertoe angles for footprint-based verification has shown to be less powerful than other geometric and texture-based approaches. Choosing almost identical FMR and FNMR, Fig. 13 indicates that rates for the ToeLength feature are as high as 26.75% and 26.56%, respectively. Due to close-fitting toes at the absence of pegs, intertoe valleys could not be detected correctly in many cases.

Good performance results, especially for low FMR at acceptable FNMR could be obtained using the Minutiae algorithm. Its matching accuracy of FMR 1.35% and FNMR 4.06% is similar to the Eigenfeet feature, but requires higher resolution to correctly identify ridges and minutiae. However, genuine matching scores returned by BOZORTH3 are lower than fingerprint acceptance thresholds recommended by NIST [12], possibly caused by the higher number of minutiae (300-400 per ballprint in contrast to 40-100 per fingerprint).

Last, the local width-based Shape feature also performed well for footprint-based verification. It exhibits an FMR of 6.13% at FNMR 5.31%, which is slightly worse than the Eigenfeet feature, but still acceptable.

If we combine matching results of the three best algorithms – Eigenfeet, Minutiae and Shape – recognition

Algorithm	Threshold	FMR	FNMR
Silhouette	51	28.91%	29.38%
Soleprint	62	19.5%	20.94%
Eigenfeet	69	2.52%	2.18%
ToeLength	52	26.75%	26.56%
Minutiae	6	1.35%	4.06%
Shape	90	6.13%	5.31%

TABLE II: Comparing recognition performance scores

Algorithm	FMR	FNMR
Fusion at decision level	0.95%	1.88%
Fusion at matching score level	1.05%	1.25%

TABLE III: Improvement of accuracy using fusion techniques

accuracy can further be improved (see Table III). We employ information fusion at the decision level using majority vote and at the matching stage using a sum rule. In the first case, single reported matching scores using the thresholds in Table II are combined using the class voted by the majority of single biometric classifiers. The second technique assigns (equal) weights to each modality and computes a sum of individual matching scores.

Presumably, looking at the results about matching performance in Fig. 13 and error rates in Tables II and III, three main results are obtained:

1. Experimental results show that matching performance is split into two classes. In case of the better performing algorithms Eigenfeet, Minutiae and Shape, EERs of approximately 2 to 6% are achieved, while Silhouette, Soleprint and ToeLength show EERs of 20-30%.
2. The Eigenfeet algorithm is the feature of choice if only low-resolution input is available.
3. Combining Eigenfeet, Minutiae and Shape can further improve matching accuracy ( $\approx 1\%$  EER).

### C. Impact on Real-World Setups

Footprint-based biometric verification for a population size of 32 is shown to be theoretically applicable in environments where user-friendly and accurate data acquisition can be achieved. Exhibiting correct classification rates of up to 99%, the proposed system outperforms first existing attempts on personal recognition or identification using footprints [11] with recognition rates of 85%. However, its operation in *identification mode* instead of *verification mode*, i.e., matching is executed against all templates in the database and not against a claimed identity template, is not yet analyzed and subject to further

inspection. It is clear that for commercial applications (such as access control in wellness domains, spas or thermal baths), this might be an important issue. Additionally, larger time lapses between recordings of samples or different recording conditions (wet feet) deserve further attention. For traditional access control, where highest reliability and accessibility is required (and no privacy issues exist), it is better to stick to classical fingerprint, iris or face biometrics. But footprints are suitable for restricted area access-control in, e.g., public baths, when high accessibility is achieved due to the absence of socks and closed shoes. As [11] suggested for Japanese apartments, if a sensor is placed on the entrance floor of restricted areas where people step without shoes, footprints can be obtained without the need for cooperation. Last, its use in multimodal biometric systems, when different biometrics are combined, is promising.

## VI. SUMMARY

We have proposed a footprint-based biometric verification system employing six geometric, shape-based and texture-based features, partly derived from hand, face, and fingerprint biometrics [7, 12, 16] and have compared their accuracy performance.

The incorporated Eigenfeet feature based upon PCA showed the best results with 2.52% FMR and 2.18% FNMR. But also the application of minutiae-based or

shape-based features provided reasonable recognition accuracy. We have experienced problems employing feature extraction using edge-detection on the sole of the foot due to creases at different rotations of the foot. The extraction of toe lengths and inter-toe angles turned out to be a difficult task and together with the Silhouette feature comparing foot silhouettes all three algorithms with EERs exceeding 20% are not suited for commercial applications. With fusion techniques [13] recognition accuracy could further be improved (EERs of approx. 1%).

The proposed approach has the advantage of being image-based, and no special hardware is required to capture footprints. However, the impact of water on footprint-based recognition (e.g., for its use in thermal baths) and dependency on recording times has yet to be studied. Recapitulating, using footprint-based personal recognition might be the biometric identifier of choice when three conditions hold: (1) the environment guarantees the clean and comfortable capture of footprints, (2) no high security is demanded, and (3) users claim a need for noninvasive identifiers in the sense of privacy issues.

## Acknowledgments

We would like to thank Michael Gschwandtner for the idea and source code of the Shape feature.

- 
- [1] J. Canny. A computational approach to edge detection. *IEEE Transactions on Pattern Recognition and Machine Intelligence*, 8(6):679–698, Sept. 1986.
  - [2] P. Gejguš and M. Šperka. Face tracking in color video sequences. In K. I. Joy and L. Szirmay-Kalos, editors, *Proceedings of the 19th spring conference on Computer graphics (SCCG'03)*, pages 245–249, New York, NY, USA, 2003. ACM Press.
  - [3] A. K. Jain, A. Ross, and S. Prabhakar. An introduction to biometric recognition. *IEEE Transactions on Circuits and Systems for Video Technology*, 14(1):4–20, 2004.
  - [4] J.-W. Jung, K.-H. Park, and Z. Bien. Unconstrained person recognition method using static and dynamic footprint. In *Proceedings of the 18th Hungarian-Korean Seminar*, pages 129–137, 2002.
  - [5] J.-W. Jung, T. Sato, and Z. Bien. Dynamic footprint-based person recognition method using a hidden markov model and a neural network. *International Journal of Intelligent Systems*, 19(11):1127–1141, 2004.
  - [6] R. B. Kennedy. Uniqueness of bare feet and its use as a possible means of identification. *Forensic Science International*, 82(1):81–87, 1996.
  - [7] A. Kumar, D. Wong, H. Shen, and A. Jain. Personal verification using palmprint and hand geometry biometric. In J. Kittler and M. Nixon, editors, *Proceedings of AVBPA*, volume 2688 of *LNCS*, pages 668–678. Springer Verlag, 2003.
  - [8] A. Kumar and D. Zhang. Combining fingerprint, palmprint and hand-shape for user authentication. In *Proceedings of the 18th International Conference on Pattern Recognition (ICPR'06)*, pages 549–552. IEEE Computer Society, 2006.
  - [9] D. Morton. Metatarsus atavicus: the identification of a distinct type of foot disorder. *The Journal of Bone and Joint Surgery*, 9(5):531–544, 1927.
  - [10] C. S. Myers and L. R. Rabiner. A comparative study of several dynamic time-warping algorithms for connected word recognition. *The Bell System Technical Journal*, 60(7):1389–1409, 1981.
  - [11] K. Nakajima, Y. Mizukami, K. Tanaka, and T. Tamura. Footprint-based personal recognition. *IEEE Transactions on Biomedical Engineering*, 47(11):1534–1537, 2000.
  - [12] National Institute of Standards and Technology. Fingerprint Image Software 2, 2006. <http://fingerprint.nist.gov/NFIS>.
  - [13] A. Ross and A. K. Jain. Information fusion in biometrics. *Pattern Recognition Letters*, 24(13):2115–2125, 2003.
  - [14] R. Sanchez-Reillo, C. Sanchez-Avila, and A. Gonzalez-Marcos. Biometric identification through hand geometry measurements. *IEEE Transactions on Pattern Analysis and Machine Intelligence*, 22(10):1168–1171, 2000.
  - [15] K. Sobottka and I. Pitas. Extraction of facial regions and features using color and shape information. In *Proceedings of the 13th International Conference on Pattern Recognition (ICPR'96)*, pages 421–425, 1996.

- [16] M. Turk and A. Pentland. Eigenfaces for recognition. *Journal of Cognitive Neuroscience*, 3(1):71–86, 1991.
- [17] E. Yörük, H. Dutagaci, and B. Sankur. Hand biometrics. *Image and Vision Computing*, 24(5):483–497, 2006.
- [18] E. Yoruk, E. Konukoglu, B. Sankur, and J. Darbon. Shape-based hand recognition. *IEEE Transactions on Image Processing*, 15(7):1803–1815, 2006.

### Biographies

**Andreas Uhl** is an associate professor at the Computer Sciences Department of the University of Salzburg (Austria), where he leads the Multimedia Signal Pro-

cessing and Security Lab. He is also lecturer at the Carinthia Tech Institute and the Salzburg University of Applied Sciences. His research interests include image and video processing, wavelets, multimedia security, biometrics, parallel algorithms, and numbertheoretical numerics.

**Peter Wild** received a bachelor's degree from the Department of Computer Sciences at the University of Salzburg (Austria), where he is currently finishing his master's thesis in the area of biometrics. He is also a referee at the Salzburg Institute of Education.